Molecular Structure Elucidation of a New Anhydrous Polymorph of Acyclovir: Experimental and Computational Approach

CARMEN TRIPON[1]*, IRINA KACSO[1], MARIA MICLAUS[1,2], XENIA FILIP[1], IOAN BRATU[1], CLAUDIU FILIP[1]

[1] National Institute for Research and Development of Isotopic and Molecular Technologies, 65-103 Donath Str., 400293, Cluj-Napoca, Romania

[2] Babes-Bolyai University, 1 Kogalniceanu Str., 400084, Cluj-Napoca, Romania

We present the spatial architecture of a new anhydrous polymorph of Acyclovir, obtained by rapid evaporation of a solution composed of Acyclovir and methanol. X-ray powder diffraction (XRPD), solid-state NMR (SS-NMR), differential scanning calorimetry (DSC), and FTIR spectroscopy have been used as experimental tools to prove the formation of this new solid form and to characterize its crystalline packing. Hereby, we determined that the asymmetric unit of this polymorph consists of two non-equivalent Acyclovir molecules, linked by hydrogen-bonds. The good correlation between the experimental ^{13}C NMR chemical shifts and those predicted by molecular modeling confirms the molecular model proposed by XRPD refinement.

Keywords: Acyclovir; polymorphism; crystalline structure

The rapid progress of the parallel crystallization technology made in the last decade has facilitated the solid form screening of active pharmaceutical ingredients (APIs), increasing the demand for elucidating the crystalline packing of these new solid forms. Solving the structure is a first step in selecting those compounds with adequate physico-chemical properties, which made them potential candidates for the so called drug design process. Besides single crystal X-ray diffraction, which generally is able to solve the molecular structure by itself, in those cases when single crystals cannot be grown the already well established NMR assisted crystallography protocol is successfully used to determine the molecular architecture in powders. This protocol which combines X-ray powder diffraction (XRPD) with complementary techniques such as solid-state NMR (SS-NMR) and molecular modeling (MM), is able to facilitate the selection of the accurate structure solution in a relatively short time [1-7]. ^{13}C solid-state cross polarization under magic angle spinning (CP/MAS) NMR spectra of natural abundance compounds provide initial structural information regarding the number of molecules in the asymmetric unit, the presence of a polymorphs mixture, as well as an overview on the molecular dynamics in the lattice. Another NMR key information is obtained from an inspection of the ^{13}C chemical shifts, since it is known that a change in the atoms packing mode is reflected by sometimes severe chemical shifts displacements. Subsequently, all these information are introduced in the XRPD refinement procedure and finally lead to the selection of the optimum crystal structure, for which the experimental and calculated chemical shifts are in good agreement [8-11].

In this work, we applied the NMR assisted crystallography protocol to elucidate the molecular architecture of a polycrystalline anhydrous form of Acyclovir (ACV-form II), which was previously reported [12], but whose structure remained unknown. The commercial form of Acyclovir (ACV-form I), crystallize in the monoclinic space group $P2_1/n$, with the following unit cell parameters: a=25.459(1) Å, b=11.282(1) Å, c=10.768(1) Å, and β=95.16(1)°. The asymmetric unit contains three molecules of ACV and two molecules of water [13].

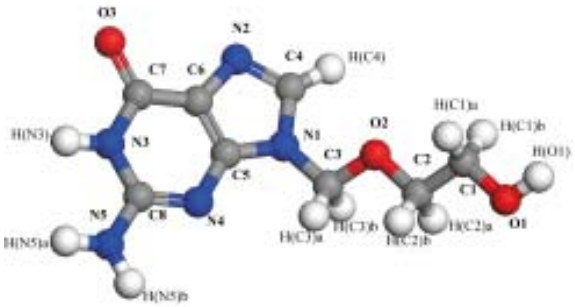

Fig. 1. Acyclovir molecule ($C_8H_{11}N_5O_3$)

Acyclovir (fig.1) is well known for its antiviral activity on herpes simplex viruses (such as HSV-1 and HSV-2), human herpes virus (HHV-6), and varicella zoster virus (VZV). Various studies have been made regarding the absorption of ACV in the human body, all of them showing its poor absorption due to its reduced solubility in aqueous media [14]. The bioavailability of ACV after oral administration spans between 10% to 30%, approximately 80% of an oral dose being excreted through the kidneys. During the last years, many attempts to improve the oral bioavailability of ACV have been made, including its complexation with cyclodextrins [15], oral-microemulsions [16], solid dispersion with polyethylene glycol - PEG 6000 and polyvinylpyrrolodone PVP K 30 [17], co-crystals between ACV-tartaric acid and ACV-citric acid [18], and dipeptide prodrugs [19].

The present paper, describes our work on elucidating the molecular architecture of the anhydrous form of Acyclovir recrystallized from methanol (ACV – form II), by applying an experimental protocol which combines several techniques, such as X-ray powder diffraction, solid-sate NMR and FTIR spectroscopy, differential scanning calorimetry (DSC), and molecular modeling.

Experimental part

Preparation of ACV-form II

Acyclovir and methanol were purchased from commercial sources (TCI - TOKYO CHEMICAL INDUSTRY

* *email: carmen.tripon@itim-cj.ro; Tel.: +4 0264 584037*

CO., LTD.) and used as received. Commercial Acyclovir, ACV-form I, is a hydrate form, containing three molecules of ACV and two molecules of water. ACV- form II was obtained starting from a solution containing 50 mg Acyclovir dispersed in 70 mL methanol. Afterwards, this solution was heated at 68°C in a closed container until total dissolution. The solvent was rapidly evaporated on the same temperature [12].

Differential Scanning Calorimetry

The experiments were carried out with a Shimadzu DSC-60 differential scanning calorimeter using Shimadzu TA-WS60 and TA60 2.1 version system software for data acquisition and analysis. Non hermetic aluminum pans were used to perform the experiments, in which 1–2 mg of sample were accurately weighed, and then sealed with the lid. The samples were heated starting from the ambient temperature up to 350°C under flowing nitrogen flux, with a heating rate of 10°C /min.

X-ray Powder Diffraction

XRPD measurements were performed at room temperature on a Bruker D8 Advance powder diffractometer using Cu Kα1 radiation (λ= 1.54056 Å). The θ–2θ Bragg–Brentano configuration geometry and incident-beam Ge (111) monochromator were used. The sample was ground to a fine homogeneous powder using an agate pestle and mortar and mounted in a sample holder. The measurements were performed in the 3–40° range in steps of 0.01°.

Infrared spectroscopy

FTIR spectra were registered in the 4000-400 cm^{-1} spectral range with a resolution of 4 cm^{-1} using a JASCO 6100 spectrometer by employing KBr pellet technique.

Solid-State NMR spectroscopy

^{13}C solid state cross-polarization magic-angle-spinning (CP/MAS) NMR spectra were recorded at 500 MHz ^{1}H Larmor frequency with a Bruker AVANCE III WB UltraShield Plus spectrometer. The SS-NMR experiments were performed on ACV-form I and ACV-form II at room temperature. Standard ^{13}C CP/MAS experiments were performed at a spinning frequency of 15 kHz, and the duration of the ^{1}H 90° pulse was 2.3μs. The spectra were acquired under two-pulse phase-modulated (TPPM) ^{1}H decoupling at 100 kHz by averaging 800 scans, with a recycle delay of 30 s, and 1 ms contact pulse. ^{13}C CP/MAS spectra of both ACV- form I and ACV-form II are calibrated according to the $^{13}CH_3$ line in TMS through an indirect procedure which uses as an intermediary standard the ^{13}C SS-NMR resonance line of the carboxyl group in glycine (176.5 ppm). ^{1}H NMR spectrum of ACV-form II was obtained in the ultra-fast spinning regime, i.e. ν_R=60 kHz, using a state-of-the-art 1.3 mm double resonance probehead, and was calibrated to the adamantane resonance line (1.2 ppm).

Computational methods

All the computational tasks, ranging from XRPD structure determination, to calculations based on MM and *ab initio* methods, were performed using an integrated software package, Accelrys Materials Studio® (MS) suite [20].

First-principles geometry optimization and NMR chemical-shift calculations were performed using the MS CASTEP and MS NMR CASTEP tools. CASTEP implements density functional theory (DFT) within a generalized gradient approximation and the planewave pseudo-potential approach [21]. All calculations used the PBE exchange-correlation functional and ultrasoft pseudo-potential. The XRPD crystal structure solutions have been optimized prior to shielding calculations in two different ways: (i) the positions of the heavy atoms and unit cell parameters were kept fixed at their diffraction derived values, but the hydrogen atoms were allowed to move (the H-relaxed case), and (ii) by fixing only the unit cell parameters and allowing the positions of all atoms to be optimized (the all-relaxed case), respectively. A comparison of the average forces remaining on the atoms after geometry optimization was carried out using a maximum planewave cutoff energy of 610 eV. When constrained, the heavy atoms were still affected by average forces (given as Cartesian components) of ~ 0.99 eV/Å(C), ~ 1.28 eV/Å(N) and ~ 0.58 eV/Å(O) as compared to ~ 0.001 eV/Å(H), indicating that further relaxation was necessary. In the case when the heavy atoms were also relaxed, average forces of similar order of magnitude were determined for all atomic species, ranging between 0.001 eV/Å(H) and 0.003 eV/Å(N).

The NMR shielding parameters were computed using the Gauge-Including Projector Augmented-Wave (GIPAW) method [22-23]. For calculation of the shielding tensors a planewave basis set was employed with a cutoff energy of 610 eV, with integrals taken over the Brillouin zone using a Monkhorst-Pack grid of minimum sample spacing 0.04 $Å^{-1}$, and ultrasoft pseudopotentials generated on the fly.

Results and discussions

DSC

Differential scanning calorimetry (DSC) measurements reveal information on the thermal behaviour of the ACV-form I and ACV-form II, as summarized in table 1. The endothermic peaks are identified during the dehydration and melting processes, the entire peak area being used to calculate the enthalpy of various thermal effects. DSC curve of ACV-form I revealed three endothermic events: a broad signal between 85-105°C with peak maxima at 91°C and ΔH= -14.35 kJ/mol, due to the loss of water molecules, and another one between 168-180°C with ΔH= -0.95 kJ/mol, corresponding probable to the solid-solid transformation [24]. A sharp endothermic peak appears between 257-262°C, with maxima at 259.5°C and ΔH= -36.66 kJ/mol, which corresponds to the melting of the drug, followed by decomposition. ACV-form II presents only one thermal event between 258-262°C, with maxima centered at 259.6°C and ΔH= -38.51 kJ/mol, due to the melting of the sample. The missing of the endothermic signal characteristic to the loss of water indicates that this form is anhydrous. The DSC curves of the two forms of ACV are illustrated in figure 2.

Analysis of XRPD data

At a primary inspection of the XRPD patterns of the starting ACV-form I and its anhydrous polymorph ACV-form II, important differences between the two forms of Acyclovir can be noticed, as shown in figure 3.

The crystal structure determination of ACV-form II from the XRPD data was performed with *MS Reflex Plus* program. The first 27 peaks were chosen for indexing the powder pattern using the Treor algorithm. Indexing was followed by an automated search for the most probable space group based on the systematic absences of Bragg reflections in the experimental powder pattern: the best solution corresponds to the $P2_12_12_1$ space group.

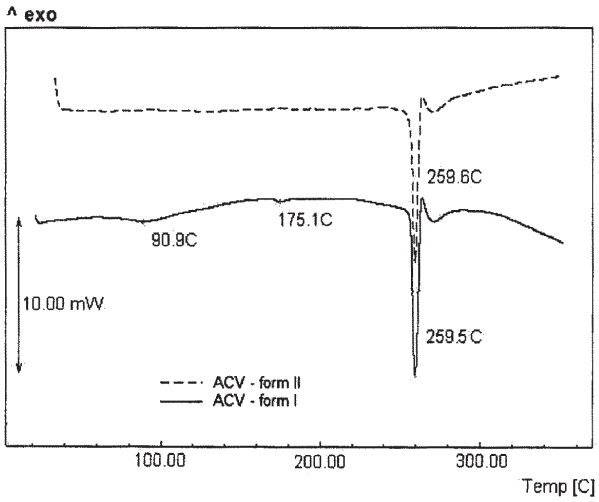

Fig. 2. DSC curves of ACV-form I (continuous line) and ACV-form II (dashed line)

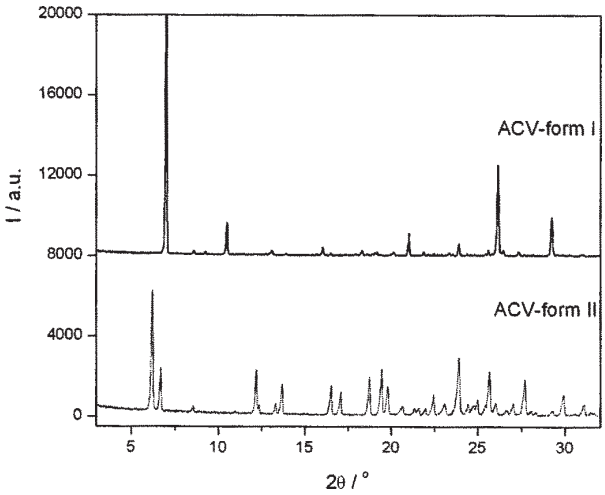

Fig. 3. X-ray powder diffraction patterns of ACV-form I (up) and ACV-form II (bottom)

	ACV-form I			ACV-form II
T onset (°C)	85.2	168.1	257.6	258
T peak (°C)	90.9	175.1	259.5	259.6
T endset (°C)	104.6	179.6	262.4	262
Heat (kJ/mol)	-14.35	-0.95	-36.66	-38.51

Table 1
THERMOANALYTICAL DATA OF ACV-FORM I AND ACV-FORM II

Next, we carried out the Pawley refinement of the XRPD pattern, where the cell parameters were also optimized. A pseudo-Voight profile function was considered and a set of characteristic pattern, and sample parameters were simultaneously refined until the value of the associated FOM reached their minima, R_{wp} ~ 8.6 (Rp ~ 6.4). Subsequently, the ACV-form II molecular structure was built from scratch using the MS editing tool. According to the ^{13}C CP/MAS SS-NMR spectrum (see a detailed description on the Solid-State NMR spectroscopy section), there are two molecules in the asymmetric unit: thus, a dimmer was considered for geometry optimization with *MS Forcite Plus* at the molecular mechanics level, and the resulted supramolecular structure was used then as a starting model to determine the preliminary crystal structure solution. The Powder Solve package was used to constantly adjust the conformation, position and orientation of the molecules in the unit cell, in order to maximize the agreement between the calculated and the measured diffraction data. For this purpose, a direct-space search method based on the Simulated Annealing algorithm was employed by considering 10 degrees of freedom, for each of the two non-equivalent molecules in the asymmetric unit: six related to the molecular position and orientation, whereas the remaining four are the independent flexible torsion angles of the ACV molecule shown in figure 1 (C5-N1-C3-O2, N1-C3-O2-C2, C3-O2-C2-C1, O2-C2-C1-O1). The solution was systematically searched by applying a close contact penalty function of 0.5 in 5 cycles, with $9.5x10^8$ steps/cycle.

The structural model obtained with the best fit factor was taken as input for Rietveld refinement. Besides the parameters considered previously, the hydrogen positions were also varied during this refinement stage. Finally, the crystal structure solution was obtained with an R_{wp} = 10.78% (R_p =8.02%) fit factor. To model the XRPD pattern

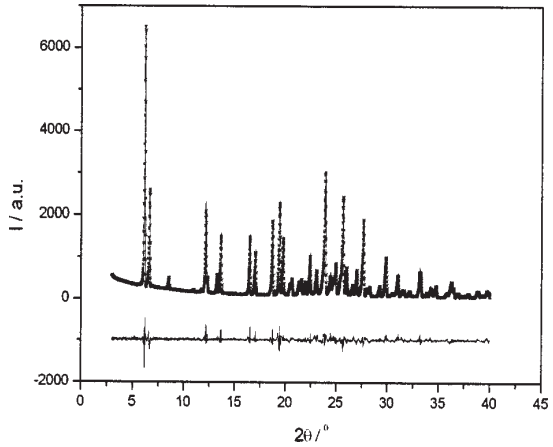

Fig. 4. Rietveld plot for ACV-form II, where the experimental pattern is represented by black symbols, the calculated pattern with continuous line, and the difference pattern is illustrated in the bottom

the Pseudo-Voigt profile function was chosen with the U,V,W Caglioti parameters being refined. The zero point and lattice parameters were refined separately. The asymmetric profile was modeled by Berar-Baldinozzi correction. Preferred orientation was taken into account by March-Dollase function. Background was approximated by a polynomial of order 20. After Rietveld refinement the cell parameters which were obtained are given in table 2.

Since XRPD analysis cannot provide the hydrogen positions with sufficient accuracy, a geometry optimization was performed as described in the *Computational methods* section. As a consequence of the geometry optimization using the all-relaxed case, it results that the two molecules that composed the asymmetric unit of ACV-form II are linked by the following hydrogen bonds: H-$(N5a,b)_A$···$O2_B$ (2.9 Å), H-$(N5a,b)_A$···$O3_B$ (2.8 Å), $N4_A$···H-$(O1)_B$ (2.8 Å), $N2_A$···H-$(N5a,b)_B$ (2.9 Å), H-$(N3)_A$···$N2_B$ (2.7

Compound:	**ACV – form II**
Chemical formula:	**$C_8H_{11}N_5O_3$**
Crystallographic system:	**Orthorhombic**
Space group:	**$P2_12_12_1$**
Lattice parameters (Å):	**a=28.829(5), b=15.089(9), c= 4.551(3)**
Volume (Å^3):	**1981.270**
Z:	**4**
Radiation type:	**Cu Kα_1, λ=1.54056 Å**
Data collection mode:	**Reflection**
Scan method:	**Continuous**
2θ values (°):	**$2\theta_{min}$= 3; $2\theta_{max}$= 40; $2\theta_{step}$=0.01**
R factors and goodness-of-fit:	**R_{wp} = 10.78% ; R_p =8.02%**
No. of data points:	**3518**
No. of positional parameters:	**102**
No. of restraints:	**76**

Table 2
CRYSTALLOGRAPHIC DATA FOR ACV – FORM II AND REFINEMENT INFORMATION

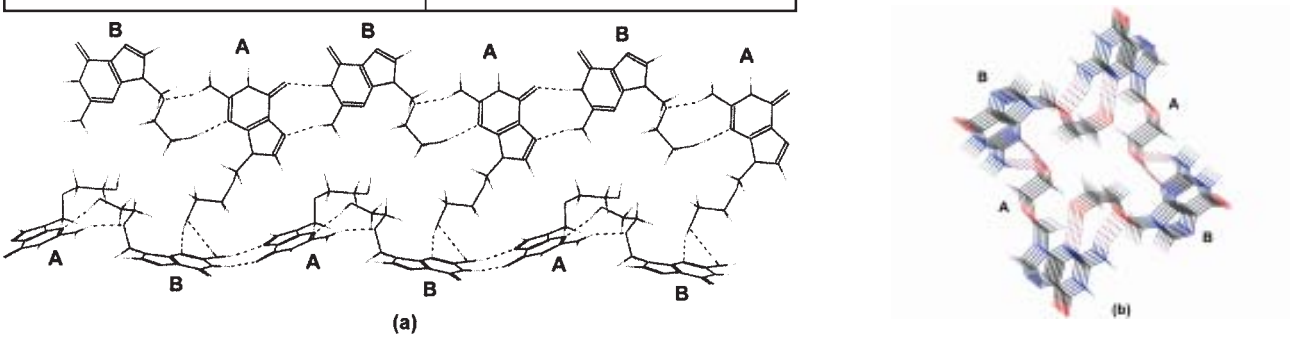

Fig. 5. Supramolecular arrangements in the crystal lattice of ACV-form II along to a direction close to *a* crystallographic axis **(a)**, and *b* crystallographic axis **(b)**, respectively

A°), $O3_A$···H-$(N3)_B$ (2.7 A°). The hydrogen bonding network and the crystal packing patterns induced by these non-covalent interactions in ACV-form II are emphasized in figure 5(a-b).

The major conformational differences between the two non-equivalent acyclovir molecules A and B in the crystallographic asymmetric unit consist on the values of the following torsion angles, as illustrated in figure 6 and detailed in table 3.

FTIR Spectroscopy

FTIR spectra of ACV-form I and ACV-form II are presented in figure 7 (**a-c**). Based on literature data [25], a series of experimental IR frequencies and their assignments are presented.

In the case of ACV-form I, in the 3500-3300 cm^{-1} spectral region (fig.7 **a**) two bands located at 3469 and 3520 cm^{-1} are identified, which correspond to primary and secondary amines [18].

In the same spectral range of ACV-form II, the following spectroscopic assignments can be made: 3371 cm^{-1} – νOH; 3207 cm^{-1} –$\nu_{assym}NH_2$; 3182 cm^{-1} –$\nu_{sym}NH_2$; 2714 cm^{-1} –νNH. The IR absorption located at 3371 cm^{-1} indicates that the OH group (O_1 in fig. 1) situated at the aliphatic extremity of ACV-form II is involved in a hydrogen bond. In the 3600-3000 cm^{-1} spectral domain NH and CH stretching vibrations can be found: CH of alkenes (3100-3000 cm^{-1}), and CH of alkanes (~3000 cm^{-1}) [25]. The band located at ~3100 cm^{-1} can be assigned to =C-H stretching vibrations [26].

In the next spectral region (1800-1500 cm^{-1}) (fig. 7 **b**) the two bands located at 1716 cm^{-1} for ACV-form I and 1701 cm^{-1} for ACV-form II can be assigned to [$\delta(NH_2)$+δ(NH)] –*in phase* and *out-of-phase*, respectively [27]. Also, the following assignments for ACV-form I are observed: 1693 cm^{-1}-αC=O; 1632 cm^{-1}-δNH_2, 1610 and 1573 cm^{-1}-δNH [24]. The band at 1584 cm^{-1} belongs to C=C symmetric stretching vibration of aromatic ring of

Torsion angle (°)	Molecule A	Molecule B
N1-C3-O2-C2	-167	101
C3-O2-C2-C1	-73	90
O2-C2-C1-O1	159	64

Table 3
TORSION ANGLES INSIDE THE ACYCLOVIR NON-EQUIVALENT MOLECULES A AND B, FOR THE GEOMETRICALLY OPTIMIZED STRUCTURE OBTAINED USING THE ALL-RELAXED CASE

Fig. 6. Superposition of the two non-equivalent molecules in the asymmetric unit of ACV-form II (A and B), revealing the major structural differences related to the conformations of the aliphatic fragment

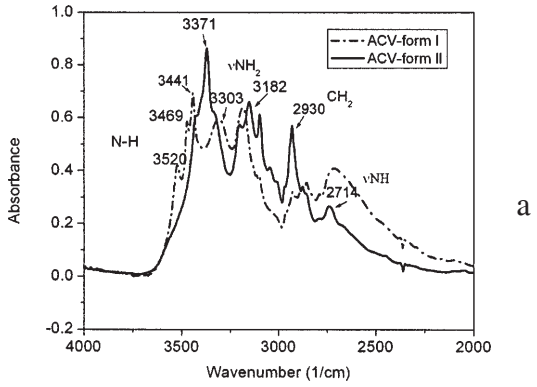

a

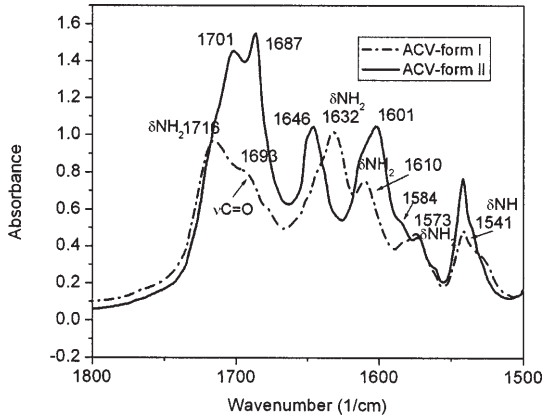

b

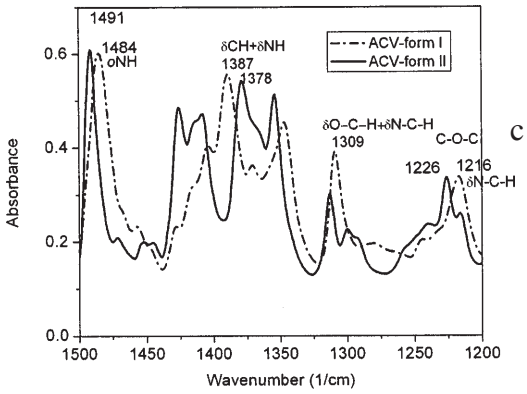

c

Fig. 7. FTIR spectra of ACV-form I (dashed line) and ACV-form II (continuous line), **(a)** 4000-2000 cm^{-1} spectral range; **(b)** 1800-1500 cm^{-1} spectral range; **(c)** 1500-1200 cm^{-1} spectral range

ACV-form II [28]. The bands located at 1610 and 1599 cm^{-1} in ACV-form I spectrum, assigned to NH_2 and to NH bending vibration are shifted to 1601 cm^{-1} and 1592 cm^{-1} respectively, in the ACV-form II FTIR spectrum. This shift indicates that the NH_2 and NH groups are involved in hydrogen bonds [18].

The band located at 1387 cm^{-1} in the ACV-form I spectrum can be assigned to δ(NH) vibrations [27]. This band is shifted to 1378 cm^{-1} in the IR spectrum of ACV-form II, due to the formation of a hydrogen bond which involves the NH group from the ring (N_3 in fig. 1). In the same spectral region (1500-1200 cm^{-1}) (fig. 7 **c**), C-O-C

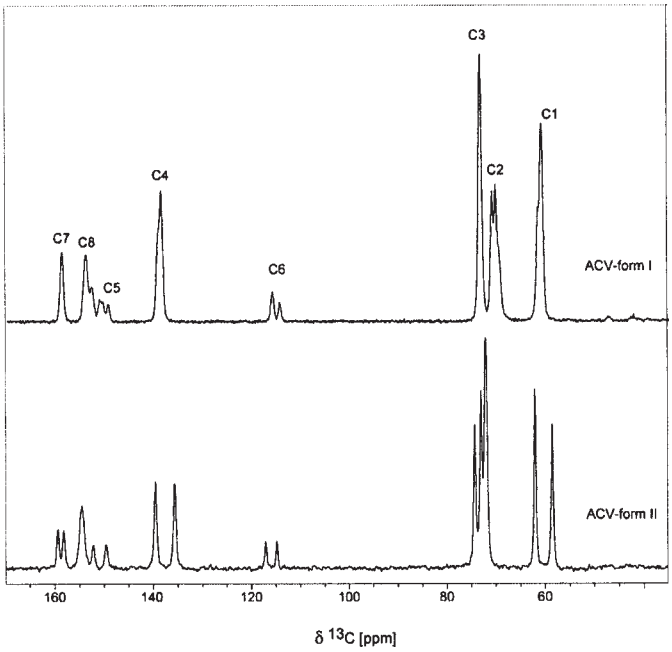

Fig. 8. ^{13}C CP/MAS NMR spectra of ACV-form I and ACV-form II

Table 4
EXPERIMENTAL AND COMPUTED ^{13}C CHEMICAL SHIFTS ON THE SPECIFIED CRYSTAL STRUCTURE MODEL OF ACV – FORM II

C site	$\delta^{exp}(^{13}C)$ [ppm]	$\delta^{calc}(^{13}C)$ [ppm]
$C1_A$	58.52	55.76
$C1_B$	62.05	61.21
$C2_A$	74.31	76.19
$C2_B$	73.01	75.67
$C3_A$	72.04	74.4
$C3_B$	72.04	72.05
$C4_A$	135.61	136.66
$C4_B$	139.63	141.09
$C5_A$	149.67	149.78
$C5_B$	152.18	149.98
$C6_A$	117.07	118.47
$C6_B$	114.79	117.47
$C7_A$	158.21	156.82
$C7_B$	159.40	158.14
$C8_A$	154.52	150.95
$C8_B$	154.52	153.32
RMSD		**1.93**

stretching frequency appears in the 1200-1270 cm^{-1} spectral range [29,30].

Solid-state NMR – Experimental and computed ^{13}C chemical shifts

The ^{13}C CP/MAS NMR spectra of both ACV-form I and ACV-form II are shown in figure 8, where the assignment of each line was obtained by MS NMR CASTEP calculations as described in Computational methods section. As first reported in the literature [13], the asymmetric unit of ACV-form I encloses three molecules, two of them in *gauche* conformation, and one in *trans* conformation. This is illustrated in the ^{13}C CP/MAS NMR spectrum of ACV-form I, where each of the eight carbons in the molecule are represented by double-split resonance lines corresponding to two different conformations, with one exception, namely C3 carbon, where the two lines overlap due to resolution limitations. The eight chemically distinct carbon sites in the molecule of ACV-form II are represented by double resonances, which indicates that this anhydrous

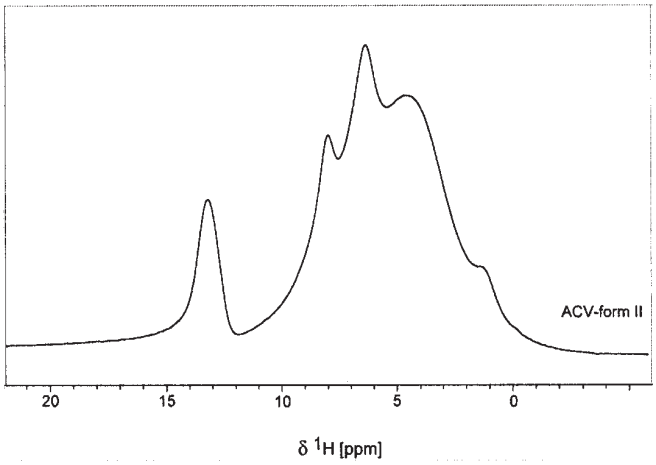

Fig. 9. ^{1}H NMR spectrum of ACV-form II, at ultra-fast spinning speed (ν_R =60 kHz)

form has two non-equivalent molecules in the asymmetric unit, the sample is not a mixture of different crystalline forms, and also that it does not contains impurities at detectable concentrations. This information obtained from a simple inspection of the spectra has been exploited during the crystal structure determination from the XRPD data. Since the resonance lines are much better separated in the spectrum of this new form, we can assume that the non-equivalence degree between the two molecules in the asymmetric unit of ACV-form II is more pronounced that in the ACV-form I case.

In the following step, the experimental ^{13}C NMR chemical shift values, $\delta^{exp}(^{13}C)$, are compared with the shifts $\delta^{calc}(^{13}C)$ computed on the structure model which results from XRPD refinement, with all atoms positions optimized (table 4). For this purpose, the isotropic shielding constants σ calculated as described in Computational methods were transformed into chemical shifts relative to TMS (for ^{13}C) by using the relationship $\delta = \sigma_{ref} - \sigma$, with the reference value $\sigma_{ref}(^{13}C) \sim 170$ ppm, extracted from the linear fit of the computed shielding constants against experimental shifts [4]. In our case, the root mean square deviation (RMSD) between δ^{ex} and δ^{calc} falls within a typical variation range of 1-4 ppm reported in literature [4,31,32], namely 1.9 ppm. Since only slight differences are observed between experimental and computed ^{13}C chemical shifts, we can conclude that the structural arrangement proposed by XRPD refinement is adequate.

However, to describe the crystalline packing inside the unit cell of ACV-form II and the H-bonds between the non-equivalent A and B molecules, further experimental data are necessary. In this context, the ^{1}H NMR line at 13.2 ppm (fig. 9) appears in a spectral region that clearly indicates the existence of a strong hydrogen bond which involves the proton from the NH group. The broad signal between 0-10 ppm comprises the NMR lines of the remaining 10 protons in the acyclovir molecule. Even though the resolution is not sufficient to fully separate the individual signals, we can assume that NH_2 and OH protons can be involved in weak hydrogen-bonds, for instance the partially resolved resonance at 8.5 ppm. Correlating this information from ^{1}H NMR with the crystalline packing proposed by XRPD analysis, we can confirm that a strong H-bond occurs between $N3_B$-$H(N3)_B \cdots O3_A$ and $N3_A$-$H(N3)_A \cdots N2_B$ atoms, which are separated by similar intermolecular distances, of approximately 2.7 A.° This assumption is supported by FTIR analysis, which confirms that primary and secondary amines, as well as the hydroxyl extremity of ACV-form II are involved in non-covalent interactions.

Conclusions

A new polymorph of the antiviral drug Acyclovir was obtained by rapid evaporation at 68°C of an Acyclovir-methanol solution. To determine the crystal structure of this new solid form, a protocol which combines X-ray powder diffraction with complementary techniques such as solid-state NMR, FTIR and molecular modeling was successfully applied. The good agreement between computed and experimental ^{13}C chemical shifts, and the correlation of ^{1}H fast-MAS NMR with FTIR data, confirmed the final structural architecture of ACV-form II. The crystalline packing is shown to be based on non-covalent interaction which involves the primary and secondary amines, and also the hydroxyl group located at the aliphatic edge of ACV-form II molecule.

Acknowledgments: This work was supported by a grant of the Romanian National Authority for Scientific Research, CNCS-UEFISCDI, project number PN-II-RU-PD-2011-3-0021. We gratefully acknowledge the Data Ceter of INCDTIM Cluj for providing computing facilities.

References

1. MCCUSKER, L. B., VON DREELE, R. B., COX, D. E., LOUER, D., SCARDI, P., J. Appl. Cryst., 32, nr.1, 1999, p. 36.
2. HARRIS, K. D. M., TREMAYNE, M., KARIUKI, B. M., Angew. Chem. Int. Ed., 40, nr.9, 2001, p. 1626.
3. ZHIGANG, P., CHEUNG, E. Y., HARRIS, K. D. M., CONSTABLE, E. C., HOUSECROFT, C. E., Cryst. Growth Des., 5, nr. 5, 2005, p. 2084.
4. HARRIS, R. K., HODGKINSON, P., PICKARD, C. J., YATES, J. R., ZORIN, V., Magn. Reson. Chem., 45, nr. S1, 2007, p. S174.
5. MIDDLETON, D. A., PENG, X., SAUNDERS, D., SHANKLAND, K., DAVID, W. I. F., MARKVARDSEN, A. J., Chem. Commun., 17, nr. 1, 2002, p. 1976.
6. ALUAS, M., TRIPON, C., GRIFFIN, J. M., FILIP, X., LADIZHANSKY, V., GRIFFIN, R. G., BROWN, S. P., FILIP, C., J. Magn. Reson., 199, nr. 2, 2009, p. 173.
7. HANGAN, A., BORODI, G., FILIP, X., TRIPON, C., MORARI, C., OPREAN, L., FILIP, C., Acta Cryst. B, 66, nr. 6, 2010, p. 615.
8. HARRIS, R. K., JOYCE, S., PICKARD, C. J., CADARS, S., EMSLEY, L., Phys. Chem. Chem. Phys., 8, nr. 1, 2006, p. 137.
9. NELSON, B. N., SCHIEBER, L. J., BARICH, D. H., LUBACH, J. W., OFFERDAHL, J., LEWIS, D. H., HEINRICH, J. P., MUNSON, E. J., Solid State Nuc. Magn. Reson., 29, nr. 1-3, 2006, p. 204.
10. TAM, C. N., COWAN, J. A., SHULTZ, A. J., YOUNG JR., V. G., TROUW, F. R., SYKES, A. G., J. Phys. Chem. B, 107, nr. 31, 2003, p. 7601.
11. TISHMACK, P. A., BUGAY, D. E., BRYN, S. R., J. Pharm. Sci., 92, nr. 3, 2003, p. 441.
12. LUTKER, K. M., QUINONES, R., XU, J., RAMAMOORTHY, A., MATZGER, A. J., J. Pharm. Sci., 100, nr. 3, 2011, p. 949.
13. BIRNBAUM, G. I., CYGLER, M., SHUGAR, D., Can. J. Chem., 62, nr. 12, 1984, p. 2646.
14. TAEK SOHN, Y., HEE KIM, S., Arch. Pharm. Res., 31, nr. 2, 2008, p. 231.
15. VON PLESSING ROSSEL, C., SEPULVEDA CARRENO, J., RODRIGUEZ-BAEZA, M., BERNABE ALDERETE, J., Quimica Nova, 23, nr. 6, 2000, p. 749.
16. KUMAR GHOSH, P., MAJITHIYA, R. J., UMRETHIA, M. L., MURTHY, R. S. R., AAPS PharmSciTech., 7, nr. 3, 2006, p. E172.
17. SACHAN, N. K., PUSHKAR, S., SOLANKI, S. S., BHATERE, D. S., World Appl. Sci. J., 11, nr. 7, 2010, p. 857.
18. MASUDA, T., YOSHIHASHI, Y., YONEMOCHI, E., FUJII, K., UEKUSA, H., TERADA, K., Int. J. Pharm., 422, nr. 1, 2012, p. 160.
19. SANTOS, C. R., CAPELA, R., PEREIRA, C. S. G. P., VALENTE, E., GOUVEIA, L., PANNECOUQUE, C., DE CLERCQ, E., MOREIRA, R., GOMES, P., European Journal of Medicinal Chemistry, 44, nr. 6, 2009, p. 2339.

20. ACCELRYS SOFTWARE INC., MATERIALS STUDIO®, Release 5.5, 2010; see a detailed description at: http://accelrys.com/products/materials-studio/index.html
21. CLARK, S.J., SEGALL, M.D., PICKARD, C.J., HASNIP, P.J., PROBERT, M.J., REFSON, K., PAYNE, M.C., Z. Kristallogr., 220, nr. 5-6, 2005, p. 567.
22. PICKARD, C.J., MAURI, F., Phys. Rev. B, 63, nr. 24, 2001, 245101, p. 1.
23. YATES, J.R., PICKARD, C.J., MAURI, F., Phys. Rev. B 76, nr. 2, 2007, 024401, p.1.
24. KRISTL, A., SRCIC, S., VRERER, F., SUSTAR, B., VOJNOVIC, D., Int. J. Pharm., 139, nr. 1-2, 1996, p. 231.
25. GAVIRA, J.M., DE LA FUENTE, M., NAVARRO, R., HERNANZ, A., J. Molec. Struct., 410-411, nr. 1, 1997, p. 425.
26. MUKHERJEE, B., PATRA, B., LAYEK, B., MUKHERJEE, A., J. Nanomed., 2, nr. 2, 2007, p. 213.
27. AGGARWAL, A.K., JAIN, S., Chem. Pharm. Bull., 59, nr. 5, 2011, p. 629.
28. PIS-DIEZ, R., PARAFON-COSTA, B.S., FRANCA, C.A., PIRO, O.E., CASTELLANO, E.E., GONZALES-BARO, A.C., J. Molec. Struct., 975, nr. 1-3, 2010, p. 303.
29. PATHAK, V.N., GUPTA, R., GUPTA, N., Indian J. Chem., 47B, nr. 8, 2008, p. 1303.
30. DUNCAN, A.B.F., GORDY, W., JONES, R.N., MATSEN, F.A., SANDORFY, C., Techniques of Organic Chemistry, Chemical Applications of Spectroscopy, **vol IX**, W. West (Ed.), Interscience Publishers New York, 1956, p. 483.
31. WU, A., ZHANG, Y., XU, X., YAN, Y., J. Comput. Chem., 28, nr. 15, 2007, p. 2431.
32. FILIP, X., BORODI, G., FILIP, C., Phys. Chem. Chem. Phys., 13, nr. 40, 2011, p. 17978.

Manuscript received: 4.06.2013